

# Reactive desorption and radiative association as possible drivers of complex molecule formation in the cold interstellar medium

A.I. Vasyunin

*Department of Chemistry, The University of Virginia, Charlottesville, Virginia, USA*

[anton.vasyunin@gmail.com](mailto:anton.vasyunin@gmail.com)

Eric Herbst

*Departments of Chemistry, Astronomy, and Physics, The University of Virginia, Charlottesville, Virginia, USA*

[eh2ef@virginia.edu](mailto:eh2ef@virginia.edu)

## ABSTRACT

The recent discovery of terrestrial-type organic species such as methyl formate and dimethyl ether in the cold interstellar gas has proved that the formation of organic matter in the Galaxy begins at a much earlier stage of star formation than was thought before. This discovery represents a challenge for astrochemical modelers. The abundances of these molecules cannot be explained by the previously developed “warm-up” scenario, in which organic molecules are formed via diffusive chemistry on surfaces of interstellar grains starting at 30 K, and then released to the gas at higher temperatures during later stages of star formation. In this article, we investigate an alternative scenario in which complex organic species are formed via a sequence of gas-phase reactions between precursor species formed on grain surfaces and then ejected into the gas via efficient reactive desorption, a process in which non-thermal desorption occurs as a result of conversion of the exothermicity of chemical reactions into the ejection of products from the surface. The proposed scenario leads to reasonable if somewhat mixed results at temperatures as low as 10 K and may be considered as a step towards the explanation of abundances of terrestrial-like organic species observed during the earliest stages of star formation.

*Subject headings:* astrochemistry – ISM – molecular processes

## 1. Introduction

Although it has been understood for some time that a combination of ion-molecule and neutral-neutral reactions can explain much of the exotic “carbon-chain” chemistry that occurs in the gas phase of cold interstellar cores, both starless and prestellar, the chemistry of hot cores, in which gaseous terrestrial (partially saturated) organic species of six or more atoms, known as “complex organic molecules”, or COMs for short, are formed at relatively high abundance, is not well understood (Herbst & van Dishoeck 2009). Well-known examples of COMs include methanol ( $\text{CH}_3\text{OH}$ ), dimethyl ether ( $\text{CH}_3\text{OCH}_3$ ), ethyl cyanide ( $\text{C}_2\text{H}_5\text{CN}$ ), and methyl formate ( $\text{HCOOCH}_3$ ). Early theories of the formation of these molecules were based on a warm gas-phase chemistry during the hot core stage, possibly preceded by a cold ice-mantle chemistry during the prior cold core stage (Brown et al. 1988; Charnley et al. 1992; Hasegawa et al. 1992; Caselli et al. 1993; Horn et al. 2004). The cold ice chemistry is thought to be dominated by reactions involving weakly-bound atoms such as hydrogen, which can diffuse at low temperatures. More recently, the chemistry occurring during the warm-up leading to the formation of a hot core has been emphasized. In this approach, the chemical synthesis of hot core molecules begins on the ice mantles of grains in cold cores, where species as complex as methanol are synthesized (Garrod & Herbst 2006). As the cold core collapses isothermally into a pre-stellar core and then begins to heat up as a protostellar core is formed, the collapsing gas and dust also increase in temperature. Starting at temperatures of approximately 30 K, the heavy species formed on the 10 K ice begin to diffuse and collide with one another, although they are mainly unreactive. Photons or energetic particles strike the dust particles and dissociate some of these heavy species into radicals, which are likely to be quite reactive. For example, methanol can be dissociated to produce the methoxy radical ( $\text{CH}_3\text{O}$ ) while formaldehyde can form the formyl radical ( $\text{HCO}$ ). These two radicals can possibly undergo what is known as a recombination reaction to form methyl formate ( $\text{HCOOCH}_3$ ).

Many other COMs are likely formed via recombination of radicals on ices during the warm-up period, as discussed by Garrod & Herbst (2006) and Garrod et al. (2008), who showed that large abundances of COMs in the gas can be achieved by the stage at which the temperature of the collapsing material has risen to 100 - 300 K, where thermal evaporation takes place. At temperatures above 30 K but below 100 K, smaller abundances of complex species formed on grains can also be produced via non-thermal desorption as long as the radical-radical recombination reactions can occur. Indeed, observations in various sources have shown that small abundances of gaseous COMs can be found in cooler sources than hot cores such as the galactic center or along the line of sight to protostars (Öberg et al. 2010). But, below about 25 K, it would appear that the diffusion of radicals on ice surfaces can no longer occur sufficiently rapidly to react to form COMs (Garrod & Herbst 2006). Thus,

based solely on the warm-up radical mechanism, one would not expect to find no molecules of this type in the gas of cold cores such as TMC-1.

Two recent observations of a number of terrestrial-type complex organic molecules in the cold prestellar cores L1689b and B1-b have excited the astrochemical community (Bacmann et al. 2012; Cernicharo et al. 2012) although some more limited work had reached similar conclusions for a variety of sources including TMC-1 regarding methanol and acetaldehyde ( $\text{CH}_3\text{CHO}$ ). New observations of other cold cores (Bacmann, private communication) also show the presence of COMs. The COMs seen in L1689b and/or B1-b include methanol ( $\text{CH}_3\text{OH}$ ), acetaldehyde ( $\text{CH}_3\text{CHO}$ ), methyl mercaptan ( $\text{CH}_3\text{SH}$ ), dimethyl ether ( $\text{CH}_3\text{OCH}_3$ ), and methyl formate ( $\text{HCOOCH}_3$ ), while smaller species include the methoxy radical ( $\text{CH}_3\text{O}$ ), detected in B1-b for the first time, the formyl radical ( $\text{HCO}$ ), formic acid ( $\text{HCOOH}$ ), ketene ( $\text{CH}_2\text{CO}$ ), and formaldehyde ( $\text{H}_2\text{CO}$ ). Of the complex species, only the production of methanol is well understood; it is formed via non-thermal desorption following the successive hydrogenation by atomic hydrogen on ice mantles of CO that is accreted from the gas (Watanabe & Kouchi 2002). In this paper, we propose and investigate a scenario for the formation of the complex terrestrial-type organic molecules methyl formate, dimethyl ether, and acetaldehyde in cold cores. We also report our results for the gas-phase abundances of ketene, formaldehyde, methoxy, and methanol. The scenario involves an enhanced rate of non-thermal desorption of selected precursor molecules (e.g. methoxy, formaldehyde, methanol) from cold ice mantles by a process known as reactive desorption, in which the exothermicity of surface chemical reactions is at least partially channeled into kinetic energy needed to break the bond of the product with the ice. The enhanced desorption rate is followed by gas-phase reactions leading to the COMs, among which are radiative association processes with rate coefficients that are still poorly understood. Extension of this approach to other COMs is certainly feasible.

The remainder of this paper is organized as follows. In Section 2 we describe our chemical model, while in Section 3 modeling results are presented and compared with observational data. Section 4 contains a general discussion, while Section 5 is a summary of our work.

## 2. Chemical model

For this study, we utilized a gas-grain chemical model with a network of gas-phase and grain-surface chemical reactions taken from that used by Vasyunin & Herbst (2013), which in turn is based on the well-established OSU astrochemical database<sup>1</sup>. The diffusive surface

---

<sup>1</sup><http://www.physics.ohio-state.edu/~eric/research.html>

chemistry is treated by the rate equation technique (Hasegawa et al. 1992), in which no distinction is made between the reactive surface of an ice mantle and the inert icy bulk of interstellar grains, which is a noticeable simplification in comparison with the structure of real multilayer interstellar ices (Vasyunin & Herbst 2013). Since the methoxy radical ( $\text{CH}_3\text{O}$ ) was detected in the cold core B1-b (Cernicharo et al. 2012), we introduced four gas-phase reactions for this species, which is produced during the hydrogenation of CO on grain mantles followed by desorption. In our network, the methoxy radical and its isomer, the hydroxymethyl radical ( $\text{CH}_2\text{OH}$ ), are not distinguished. The first two reactions are simple destruction reactions involving the abundant atoms H and O:

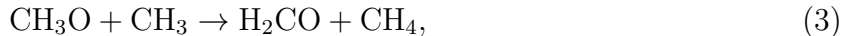


and

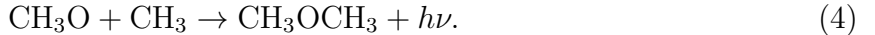


Both of these reactions have been studied to some extent in the laboratory for methoxy and hydroxymethyl radicals, as can be seen in the NIST Chemical Kinetics Database<sup>2</sup>. For the reaction with atomic hydrogen, only the process involving  $\text{CH}_2\text{OH}$  has a listed and reviewed rate coefficient, which possesses a temperature independent value of  $1.6 \times 10^{-10} \text{ cm}^3 \text{ s}^{-1}$  in the range 300-2000 K. We assume that the rate coefficient remains constant at temperatures down to 10 K in our model. For the reaction with atomic oxygen, measured and reviewed values both exist at room temperature for  $\text{CH}_2\text{OH}$  only; we assume that the average result,  $1.0 \times 10^{-10} \text{ cm}^3 \text{ s}^{-1}$ , pertains down to 10 K in our model.

The third and fourth reactions occur between the methoxy and methyl radicals:



and



The rate coefficient of reaction (3), also taken from the NIST Chemical Kinetics Database, has been measured to be  $4.0 \times 10^{-11} \text{ cm}^3 \text{ s}^{-1}$  by several investigators at room temperature and higher. We assume that this value pertains down to 10 K. Reaction (4) is a radiative association, which has not been studied in the laboratory to the best of our knowledge. The system has been studied at high density, where it essentially reaches the collisional limit at room temperature. The radiative mechanism, which is the low density process relevant to the interstellar medium, is likely to be much slower at room temperature, but to have a dependence on temperature of  $T^{-3}$  (Herbst 1980) so that by 10 K, reaction (4) is also quite

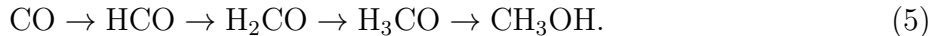
---

<sup>2</sup><http://kinetics.nist.gov/kinetics/Search.jsp>

rapid. Based on previous analyses, we estimate the rate coefficient for this reaction to be  $10^{-15}(T/300\text{ K})^{-3}\text{ cm}^3\text{ s}^{-1}$  with a large uncertainty. For convenience, information on new and other important reactions is summarized in Table 1.

The elemental abundances available for gas-grain chemistry in our simulations correspond to the EA1 set from Wakelam & Herbst (2008). These are so-called “low metal” abundances, which are lower by a factor of  $\sim 100$  for heavy elements in comparison to solar elemental abundances in order to take into account elemental depletion on grains in cold interstellar cores. The ionization rate  $\zeta$  ( $\text{s}^{-1}$ ) due to the main ionizing agent — cosmic rays — has a standard value of  $1.3 \times 10^{-17}\text{ s}^{-1}$  for molecular hydrogen. The initial abundances are all atomic except for hydrogen, which starts in the form of  $\text{H}_2$ . The gas-to-dust mass ratio is 0.01.

To treat the diffusive surface chemistry, we assume that the ice mantle surrounding interstellar grains can be represented as a two-dimensional lattice with a periodic potential. Wells of the potential are the binding sites for atomic and molecular adsorbates. Due to thermal hopping, species can move across the grain surface and react with each other. In the case of atomic and molecular hydrogen, quantum tunneling through the potential barriers is also considered as a source of surface mobility. The width of a potential barrier between two binding sites is assumed to be 1 Å. The height  $E_b$  of a barrier against diffusion for a species is assumed to be 1/2 of the desorption energy  $E_D$ . In our simulations, we consider spherical grains of a single size of  $10^{-5}\text{ cm}$  with  $\sim 10^6$  binding sites. Note that our network is inherited from previous studies in which complex organic molecules were formed at higher temperatures via diffusive surface chemistry. It contains surface radical-radical chemical reactions that lead to the formation of COMs. Since at 10 K, the mobility of molecular species on surfaces is negligible, these reactions do not contribute to the formation of COMs in this study. The only efficient diffusive reactants on grain surfaces at 10 K are atoms such as hydrogen, oxygen and nitrogen, especially atomic hydrogen, which can be an efficient tunneler. For example, hydrogen atoms that accrete onto dust particle surfaces are able to hydrogenate CO ice all the way to methanol ice at 10 K (Charnley et al. 1997; Watanabe & Kouchi 2002):



The chemistry in the gas phase is connected to grain-surface chemistry via accretion and desorption. The accretion probability for all neutral species is set to unity except for helium, for which it is taken to be zero because it is chemically inert in surface chemistry and has a very low desorption energy, so that it would thermally desorb rapidly anyway. Molecular ions are not allowed to stick on grains. There are four types of desorption included in our model: thermal evaporation (Hasegawa et al. 1992), photodesorption (Fayolle et al. 2011), desorption due to grain heating by cosmic ray bombardment (Hasegawa & Herbst 1993), and

reactive desorption (Garrod et al. 2007). In cold dark cloud cores, which are well shielded from UV radiation and have very low temperatures of  $\approx 10$  K, thermal evaporation is nil except for He, H, and H<sub>2</sub> while photodesorption can only occur slowly via photons produced by energetic electrons. Desorption due to cosmic rays has limited efficiency and has only been proven to be important on large timescales for species such as CO (Hasegawa & Herbst 1993). Constraints on the efficiency of reactive desorption, in which the products of an exothermic surface reaction are immediately ejected into the gas, are poor. To the best of our knowledge, there are no experimental constraints on its efficiency except for the case of H<sub>2</sub> (Katz et al. 1999), and only a simple statistical theory is available for larger products (Garrod et al. 2007). In this study, we consider three different efficiencies for reactive desorption: 0%, 1%, and 10% per exothermic reaction on a grain surface. The 1% efficiency is sufficient to explain observed fractional abundances of methanol ( $\approx 10^{-9}$ ) in cold cores (Garrod et al. 2007). The 10% value is equal to the highest efficiency considered by Garrod et al. (2007). Our models with these three different efficiencies for reactive desorption are labeled M0, M1, and M10.

All chemical models are run for  $10^6$  yr, which is slightly longer than so-called “early time”, at which the ion-molecule chemistry best reproduces the carbon-chain species observed in cold cores. We utilize physical conditions typical for sources such as L1689b and B1-b, where COMs were found at low temperature: T=10 K, a proton density  $n_{\text{H}}=10^5$  cm<sup>-3</sup>, and a visual extinction  $A_{\text{V}}=10$ . In our analysis, we focus on the time span  $10^5$ – $10^6$  yr.

### 3. Results

Because the calculated ice mantle composition in all three models is quite similar, we present the composition for only one model – M10 – in Figure 1. The similarity of the ice composition in all considered models arises because in this work reactive desorption affects the rates of all surface reactions by a relatively small factor of at most 10%. As such, it does not change considerably the balance between different surface chemical processes, and the resulting ice composition remains almost unchanged. As expected, our chemical model produces a typical ice composition which is similar to that calculated in a number of previous studies (Garrod & Pauly 2011; Vasyunin & Herbst 2013), and which is also generally similar to observed ice abundances towards protostars (Öberg et al. 2011). The major ice component is water, which has a nearly constant fractional abundance of  $\sim 10^{-4}$  after  $10^5$  yr. The abundances of the carbon-bearing major ice components change with time more significantly. Carbon monoxide accretes from the gas phase and at  $10^5$  yr possesses an abundance on grain surfaces similar to that of water. By  $10^6$  yr, its abundance has decreased by approximately a factor of 3 as it is gradually converted to methanol. Correspondingly, the abundances of

formaldehyde, methanol and methane rise with time by an order of magnitude or more to reach values of roughly ten to thirty percent of the abundance of water ice. Another major ice constituent observed in ices towards star-forming regions, carbon dioxide, has a very small fractional abundance of  $\sim 4 \times 10^{-7}$  in our model, despite a much larger observed abundance. This discrepancy arises because carbon dioxide is probably formed during other stages of star formation when dust grains have higher temperatures of  $\sim 20$  K (e.g., Garrod & Pauly 2011; Vasyunin & Herbst 2013).

In Figure 2, abundances of selected gas-phase species are presented for models M0, M1, and M10, with formaldehyde, methanol, and methoxy in the left panels and methyl formate, ketene ( $\text{CH}_2\text{CO}$ ), dimethyl ether, and acetaldehyde in the right panels. The upper row of panels represents results for M0 (no reactive desorption), the middle row results for M1 (1% reactive desorption efficiency), and the lower row results for model M10 (10% reactive desorption efficiency). The results for M1 are similar to those of the best-fit model in the earlier paper of Garrod et al. (2007). Fractional abundances of all these species observed in L1689b and B1-b are shown in the two rightmost columns of Table 2. We derived the observed fractional abundances in these sources by dividing the observed column densities as presented in Bacmann et al. (2012) and Cernicharo et al. (2012) by the column densities of molecular hydrogen in L1689b and B1-b. The observed fractional abundances in L1689b range from approximately  $10^{-10}$  to  $10^{-9}$  whereas those in B1-b range from approximately  $10^{-11}$  to more than  $10^{-9}$ . Given the uncertainties both in observed abundances and in our astrochemical models, we consider a model to explain successfully the observed abundance of a species if the modeled abundance differs from the observed abundance by not more than one order of magnitude (Vasyunin et al. 2004, 2008; Wakelam et al. 2010).

### 3.1. M0: a model without reactive desorption

Formaldehyde is mainly produced by the gas-phase reaction  $\text{O} + \text{CH}_3 \rightarrow \text{H}_2\text{CO} + \text{H}$ , while ketene ( $\text{CH}_2\text{CO}$ ) has two paths of formation. First, it is produced in the dissociative recombination of  $\text{C}_2\text{H}_3\text{O}^+$ , which in turn is created in the radiative association reaction between the second most abundant gas-phase molecule CO and the simple ion  $\text{CH}_3^+$ :



Secondly, ketene is produced in the neutral-neutral reaction

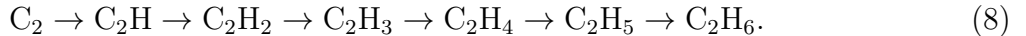


Other observed organic molecules in the model M0 have very low abundances, because they do not have gas-phase routes of formation efficient enough at 10 K to compete with accretion.

### 3.2. M1 and M10: models with reactive desorption

Our results change drastically when reactive desorption is enabled. For model M1, as can be seen in the left middle row of Figure 2, formaldehyde and methanol reach peak abundances in excess of  $10^{-9}$ , while the methoxy radical reaches a peak abundance of  $10^{-10}$ . As discussed earlier, methanol is not formed in the gas, but is formed by surface hydrogenation of CO followed by desorption (Garrod et al. 2007). This is not only true for  $\text{CH}_3\text{OH}$  but also for intermediate products of the reaction chain in eq. (5), and other products of surface reactions. As such, reactive desorption become a major source of methanol and the methoxy radical in the gas phase. The abundance of formaldehyde is affected to a lesser extent because it is already produced efficiently by gas-phase processes. The increase in the gas-phase abundances of methoxy, methanol and formaldehyde after  $3 \times 10^5$  yr is caused by the increased abundances of these species in the ice mantle, as can be seen in Figure 1.

For the molecules in the right middle panel, model M1 also shows enhanced abundances over M0. While the final abundance of ketene ( $\text{CH}_2\text{CO}$ ) increases only by a factor of three, the abundance of acetaldehyde ( $\text{CH}_3\text{CHO}$ ) is increased by four orders of magnitude, and the abundance of dimethyl ether ( $\text{CH}_3\text{OCH}_3$ ) is increased by more than ten orders of magnitude. The fractional abundances of both species with respect to hydrogen now exceed  $10^{-12}$  towards  $10^6$  yr. The additional acetaldehyde is produced via the gas-phase reaction  $\text{O} + \text{C}_2\text{H}_5 \rightarrow \text{CH}_3\text{CHO} + \text{H}$ . The  $\text{C}_2\text{H}_5$  product is ejected into the gas-phase via reactive desorption as an intermediate product of the chain of surface reactions that hydrogenate  $\text{C}_2$  into  $\text{C}_2\text{H}_6$ :



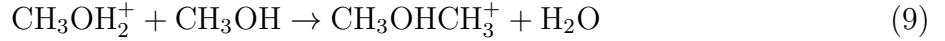
Gas-phase dimethyl ether, on the other hand, is mainly produced via the gas-phase radiative association reaction shown in eq. (4). Although inclusion of the “standard” reactive desorption with an efficiency of 1% in the model allows us to produce complex organic molecules in much higher abundances than with no reactive desorption at all, some of the predicted abundances are still quite low. For example, methyl formate ( $\text{HCOOCH}_3$ ) has an abundance in model M1 below  $10^{-14}$  in the entire time span  $10^5$ – $10^6$  yr, which is 3–4 orders of magnitude below the observed values.

The results produced by the model M10, with an efficiency for reactive desorption of 10%, are presented in the bottom row of Figure 2. In this model, the abundances of all depicted species are enhanced in comparison with model M1 and especially with model M0. In model M10, the contribution to gas-phase  $\text{H}_2\text{CO}$  from the chain of surface reactions in reaction (5) via reactive desorption is an order of magnitude larger than the gas-phase formation routes, which leads to an increase in the peak fractional abundance of  $\text{H}_2\text{CO}$  to  $6 \times 10^{-8}$ . The abundances of methoxy and methanol are increased by an order of magnitude

in comparison with model M1, and reach  $8.7 \times 10^{-10}$  and  $3.4 \times 10^{-8}$ , respectively, at their maximum.

As can be seen on the right panel in the bottom row of Figure 2, the abundances of ketene and complex organic species are increased in model M10 in comparison with model M1 by different factors. The smallest enhancement in abundance, a factor of 7 at  $10^6$  yr, is exhibited by ketene. The order of magnitude increase in the abundance of gas-phase methanol throughout the time range shown leads to an increase in the abundance of  $\text{CH}_3^+$  via the reaction  $\text{H}_3^+ + \text{CH}_3\text{OH} \rightarrow \text{CH}_3^+ + \text{H}_2\text{O} + \text{H}_2$ . The methyl ion can then react with CO in reaction (6) to produce  $\text{C}_2\text{H}_3\text{O}^+$ , and subsequently  $\text{CH}_2\text{CO}$ . An order-of-magnitude increase in the abundance of acetaldehyde is caused by the increased abundance of  $\text{C}_2\text{H}_5$ , which is ejected into the gas via efficient reactive desorption from the surface reaction chain in reaction (8).

The abundance of dimethyl ether in model M10 is increased by two orders of magnitude in comparison with model M1 because the abundances of both gaseous reactants ( $\text{CH}_3$  and  $\text{CH}_3\text{O}$ ) in reaction (4) are increased in model M10 by an order of magnitude. The increase in gaseous  $\text{CH}_3\text{O}$  derives from the increase in efficiency of reactive desorption in model M10. In turn,  $\text{CH}_3$  in model M10 is mainly produced in the gas-phase via reaction (1). Another route for the formation of  $\text{CH}_3\text{OCH}_3$  is via the dissociative recombination of protonated dimethyl ether, which is produced in the reaction of methanol with protonated methanol:

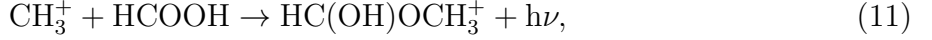


The strongest abundance enhancement in switching from model M1 to model M10 occurs for methyl formate, which increases from  $4 \times 10^{-15}$  to  $1.8 \times 10^{-12}$  at  $10^6$  yr. The most efficient gas-phase formation route for  $\text{HCOOCH}_3$  in our model is via dissociative recombination of  $\text{H}_2\text{COHOCH}_2^+$ . The principal formation route of this species occurs via the radiative association reaction (Horn et al. 2004)



The product is not normal protonated methyl formate, which has the structure  $\text{HC}(\text{OH})\text{OCH}_3^+$ . Unfortunately there is a transition state barrier between the product of reaction (10) and protonated methyl formate (Horn et al. 2004). We assume, as did Horn et al. (2004), that dissociative recombination of the product of reaction (10) can also form methyl formate + H despite the change in structure required. Reaction (10) is similar to reaction (9) in the sense that its rate depends quadratically on the abundance of gas-phase formaldehyde. Consequently, the gas-phase abundance of  $\text{HCOOCH}_3$  in the model M10 becomes comparable although still somewhat lower than the observed values at times exceeding  $3 \times 10^5$  yr. If the

dissociative recombination reaction does not lead to methyl formate, another process that can produce protonated methyl formate is the radiative association reaction (Horn et al. 2004)



followed by dissociative recombination. This reaction, however, is not as efficient in producing methyl formate in our current models.

The general behavior of models with reactive desorption is similar to that described in Garrod et al. (2007). These authors found that at  $\leq 2 \cdot 10^6$  yr, the abundances of the majority of gas-phase species are not affected significantly by the inclusion of reactive desorption. The exceptions are several hydrogenated species such as methanol and formaldehyde. In this study, we observe a similar picture extended by the enhanced abundances of COMs, descendants of  $\text{H}_2\text{CO}$  and  $\text{CH}_3\text{OH}$ , which were not considered in Garrod et al. (2007).

### 3.3. Comparison with observations

It is interesting to investigate how well our models reproduce the observed abundances of complex organic species and their precursors. To quantify the level of agreement, we calculated individual confidence parameters  $\kappa_i$  for each  $i$ -th species versus time in models M1 and M10 according to the prescription in Garrod et al. (2007) and then took the mean of the individual confidence parameters as the criterion of overall agreement. The formula for each individual confidence parameter is

$$\kappa_i = \text{erfc} \left( \frac{|\log(X_i) - \log(X_i^{\text{obs}})|}{\sqrt{2}\sigma} \right), \quad (12)$$

where  $\text{erfc}$  is the complementary error function,  $X_i$  and  $X_i^{\text{obs}}$  are the modeled and observed abundances of species  $i$  at time  $t$ , and the standard deviation  $\sigma$  is assumed to equal unity, which means that we estimate the uncertainty in observed abundances to be one order of magnitude. With this definition,  $\kappa_i$  is equal to unity when the observed and model abundances are equal, and quickly goes towards a limit of zero with increasing discrepancy between these two values. For example, when the difference is one order of magnitude,  $\kappa_i = 0.32$ , and when the difference is two orders of magnitude,  $\kappa_i = 0.046$ . Model M0 is excluded from this comparison as its results are obviously too far from observational values.

The molecules shown in Table 2 are used in the analysis. In addition to these molecules, several other simple species were observed towards B1-b and L1689b such as CO,  $\text{HCO}^+$ ,  $\text{N}_2\text{H}^+$ ,  $\text{NH}_3$ , CS and  $\text{HNCO/HCNO}$  (Hirano et al. 1999; Bacmann et al. 2002; Marcelino et al. 2009; Öberg et al. 2010). We did not include them in the comparison set for two reasons.

First, the abundances of these species come from different sets of observations, and their inclusion will make the set heterogeneous. Secondly, the abundances of these species are only slightly different in our models with and without reactive desorption. The resulting individual and mean confidence parameters for L1689b and B1-b are shown in Figures 3 and 4, respectively. For L1689b, model M1 reaches its best agreement at  $1.3 \times 10^5$  yr and model M10 at  $5.1 \times 10^5$  yr (if we exclude for M10 a small cusp at much earlier time that has a similar extent of agreement). In the case of B1-b, the time of best agreement time for model M1 is  $1.0 \times 10^6$  yr, while for model M10 it is  $2.6 \times 10^5$  yr. At these times, the average agreement is better than one order of magnitude. The individual molecular abundances at these best times are shown in Table 2. Because there are two more organic species detected in B1-b than in L1689b, we choose B1-b for detailed discussion.

At the time of best agreement for M1, the modeled abundances for the two precursor species  $\text{CH}_2\text{CO}$  and  $\text{H}_2\text{CO}$ , and the two complex species  $\text{CH}_3\text{OH}$  and  $\text{CH}_3\text{CHO}$ , out of seven species, differ from the observational values by less than one order of magnitude. For one species,  $\text{CH}_3\text{OCH}_3$ , the difference between modeled and observed abundances just slightly exceeds one order of magnitude. At the same time, model M1 somewhat overproduces methoxy and significantly underproduces methyl formate. Model M10 exhibits its best agreement with observations of B1-b significantly earlier. While it manages to reproduce the abundances of all complex organic species including  $\text{HCOOCH}_3$ , the modeled abundance of  $\text{H}_2\text{CO}$  is two orders of magnitude higher than the observed value. The abundance of  $\text{CH}_3\text{O}$  is also significantly higher than the observed value.

A possible reason for the overly high calculated abundance of methoxy in both the M1 and M10 models has been given by Cernicharo et al. (2012), who showed that on grains the isomer  $\text{CH}_2\text{OH}$  is produced more efficiently than  $\text{CH}_3\text{O}$  and released into the gas phase. This isomer has different spectral properties, and was not observed in the gas phase. The authors proposed an alternative formation route for methoxy via the gas-phase reaction



Although our chemical model currently does not discriminate between  $\text{CH}_3\text{O}$  and  $\text{CH}_2\text{OH}$ , we estimate that if methoxy is only produced by reaction (13) at its newly determined rate coefficient, then the abundance of methoxy will be in much closer agreement with observations, at least in case of B1-b. But, one must remember that since methoxy is a precursor species to complex organic molecules, lessening its abundance will also lessen the abundance of the complex molecules formed from it, especially dimethyl ether.

We show the organic abundances vs time for an altered model M10, in which the gas-phase route to methoxy is included and the reactive desorption route is removed, in Figure 5. The results can be compared with the abundances obtained with the original model M10,

which are shown in the bottom panel of Figure 2. The time of the best agreement between observed values for B1-b and results of the altered model M10 is the same as for the original model, but at later times, the level of agreement remains at almost the same value until  $10^6$  yr. For B1-b, the new fractional abundance of  $\text{CH}_3\text{O}$  at the time of best agreement is  $5 \times 10^{-11}$ , which is closer to the observed value, although still too large by an order of magnitude. This fact may imply that the rate coefficient of reaction (13) is somewhat overestimated, which is supported by older estimations. With the high value for the rate coefficient of reaction (13), the new abundance of  $\text{CH}_3\text{OCH}_3$  at the moment of best agreement for B1-b is  $1 \times 10^{-12}$ , but it increases steadily, reaching a value of  $2 \times 10^{-11}$  at  $10^6$  yr.

Finally, it is interesting to note that in B1-b the observed abundances of all organic species we consider are lower than in L1689b, including formaldehyde. If future observations confirm that this correlation is not caused by systematic errors between observational data sets, the lower abundances in B1-b argue in favor of our scenario for the formation of complex molecules in cold clouds, because our scenario implies a strong correlation between the abundances of  $\text{H}_2\text{CO}$  and COMs.

#### 4. Discussion

We have considered one approach to understanding how terrestrial-type organic molecules can be synthesized in cold starless and prestellar cores. In our approach, reactive desorption succeeds in removing precursor molecules efficiently from the ice mantles of cold dust grains into the gas, where subsequent reactions produce the organic molecules in reasonable, if not perfect, agreement with the small observed abundances detected in the cold prestellar cores L1689b and B1-b. Radiative association reactions in the gas play an important role in the synthesis of the complex organic molecules methyl formate and dimethyl ether. Both reactive desorption and radiative association reactions are still poorly understood processes in general. Moreover, the product for the proposed radiative association reaction that leads to the formation of protonated methyl formate most likely yields a different structure than desired, which may or may not form methyl formate in its lowest conformer when the ion undergoes a dissociative recombination with electrons.

Although we have discussed our model results mainly for observed COMs, our model can also be tested by its predictions for the abundances of other complex species, such as ethyl cyanide ( $\text{C}_2\text{H}_5\text{CN}$ ), which is a well-known weed in hot cores. Under cold core conditions, our model first produces ethyl cyanide in the ice mantle by hydrogenation of the  $\text{CCCN}$  radical (Hasegawa et al. 1992; Caselli et al. 1993). Reactive desorption then results in a considerable abundance of this species in the gas phase at selected times. For example, in Model M1,

the fractional abundance of ethyl cyanide peaks at over  $10^{-10}$  at a time near  $2 \times 10^5$  yr, while for Model M10, the peak value approaches a fractional abundance of  $10^{-8}$  at the same time. At the times of best agreement for models M1 and M10 with B1-b, the calculated fractional abundances of ethyl cyanide are somewhat under  $10^{-12}$  and somewhat over  $10^{-10}$  respectively, while for L1689b, these numbers are somewhat over  $10^{-10}$  and near  $10^{-11}$ .

There are perhaps other complementary approaches to the production of COMs in cold cores, where the dust surfaces are typically too cold for the surface radical-radical photochemistry suggested by Garrod & Herbst (2006). One possibility is that we are missing a large number of thermal surface/ice reactions that can occur at 10 K, typically by the diffusion of atoms somewhat heavier than hydrogen. A figure showing the many species that might be synthesized in this way was produced by S. Charnley (private communication) and can be found in Herbst & van Dishoeck (2009). Another possibility is that the dust particles are not always at 10 K, and that a variety of effects cause a temporary increase in temperature high enough to allow surface radicals to diffuse and react with one another. It is even possible that photodissociation or particle bombardment processes can cause temporary non-thermal motions of species so as to promote the rates of non-thermal diffusive reactions (Occhiogrosso et al. 2011; Kim & Kaiser 2012). Finally, tunneling from one lattice site to another for species other than atomic hydrogen will promote more rapid surface/ice reactions at lower temperatures than if the only diffusive mechanism for species heavier than H is simple thermal hopping. We hope to investigate some of these possibilities in the near future.

## 5. Summary

In this study, we have proposed and examined a scenario of formation of complex organic molecules recently found in the cold cores L1689b and B1-b with gas temperatures of 10 K. The proposed scenario is based on the assumption that complex organic species in the cold regions are formed via gas-phase ion-molecular and neutral-neutral chemistry from simpler precursors such as formaldehyde and methanol. These precursors are formed on icy surfaces of interstellar grains, and then ejected into the gas via reactive desorption. Because of our lack of knowledge of the efficiency of reactive desorption, we considered three models: M0, M1, and M10, in which the efficiency of reactive desorption per exothermic surface reaction is 0%, 1%, and 10%, respectively.

We found that the proposed scenario gives somewhat mixed agreement with observations of COMs and their precursors. Both models with non-zero reactive desorption exhibit much better agreement with observations than the model without reactive desorption. The best agreement for the whole set of species is exhibited by model M10, which possesses the

highest efficiency of reactive desorption. On the other hand, this model tends to overestimate gas-phase abundances of formaldehyde in comparison to observations by  $\sim$  two orders of magnitude. Such a discrepancy can be partly but not fully explained by uncertainties in our chemical model, particularly in the rate coefficients of chemical reactions. This fact may imply that the proposed scenario of formation of complex organic species via gas-phase reactions driven by reactive desorption is only partially responsible for the formation of these molecules, and should be assisted by other routes such as processes that warm up grains temporarily or that permit non-thermal ice reactive processes.

The authors wish to thank the anonymous referee for valuable comments, which helped us to improve the manuscript. E. H. acknowledges the support of the National Science Foundation for his astrochemistry program, and support from the NASA Exobiology and Evolutionary Biology program through a subcontract from Rensselaer Polytechnic Institute. This research has made use of NASA's Astrophysics Data System.

## REFERENCES

Anicich, V., Aeronautics, U. S. N., Administration, S., & (U.S.), J. P. L. 2003, An Index of the Literature for Bimolecular Gas Phase Cation-Molecule Reaction Kinetics, JPL Publication (Jet Propulsion Laboratory, National Aeronautics and Space Administration)

Bacmann, A., Lefloch, B., Ceccarelli, C., Castets, A., Steinacker, J., & Loinard, L. 2002, A&A, 389, L6

Bacmann, A., Taquet, V., Faure, A., Kahane, C., & Ceccarelli, C. 2012, A&A, 541, L12

Brown, P. D., Charnley, S. B., & Millar, T. J. 1988, MNRAS, 231, 409

Caselli, P., Hasegawa, T. I., & Herbst, E. 1993, ApJ, 408, 548

Cernicharo, J., Marcelino, N., Roueff, E., Gerin, M., Jiménez-Escobar, A., & Muñoz Caro, G. M. 2012, ApJ, 759, L43

Charnley, S. B., Tielens, A. G. G. M., & Millar, T. J. 1992, ApJ, 399, L71

Charnley, S. B., Tielens, A. G. G. M., & Rodgers, S. D. 1997, ApJ, 482, L203

Fayolle, E. C., Bertin, M., Romanzin, C., Michaut, X., Öberg, K. I., Linnartz, H., & Fillion, J.-H. 2011, ApJ, 739, L36

Garrod, R. T. & Herbst, E. 2006, A&A, 457, 927

Garrod, R. T. & Pauly, T. 2011, ApJ, 735, 15

Garrod, R. T., Wakelam, V., & Herbst, E. 2007, A&A, 467, 1103

Garrod, R. T., Weaver, S. L. W., & Herbst, E. 2008, ApJ, 682, 283

Gerlich, D. & Horning, S. 1992, Chemical Reviews, 92, 1509

Hasegawa, T. I. & Herbst, E. 1993, MNRAS, 261, 83

Hasegawa, T. I., Herbst, E., & Leung, C. M. 1992, ApJS, 82, 167

Herbst, E. 1980, ApJ, 241, 197

—. 1985, ApJ, 291, 226

Herbst, E. & van Dishoeck, E. F. 2009, ARA&A, 47, 427

Hirano, N., Kamazaki, T., Mikami, H., Ohashi, N., & Umemoto, T. 1999, in Star Formation 1999, ed. T. Nakamoto, 181–182

Horn, A., Møllendal, H., Sekiguchi, O., Uggerud, E., Roberts, H., Herbst, E., Viggiano, A. A., & Fridgen, T. D. 2004, ApJ, 611, 605

Karpas, Z. & Meot-Ner, M. 1989, The Journal of Physical Chemistry, 93, 1859

Katz, N., Furman, I., Biham, O., Pirronello, V., & Vidali, G. 1999, ApJ, 522, 305

Kim, Y. S. & Kaiser, R. I. 2012, ApJ, 758, 37

Marcelino, N., Cernicharo, J., Roueff, E., Gerin, M., & Mauersberger, R. 2005, ApJ, 620, 308

Marcelino, N., Cernicharo, J., Tercero, B., & Roueff, E. 2009, ApJ, 690, L27

Öberg, K. I., Boogert, A. C. A., Pontoppidan, K. M., van den Broek, S., van Dishoeck, E. F., Bottinelli, S., Blake, G. A., & Evans, II, N. J. 2011, ApJ, 740, 109

Öberg, K. I., Bottinelli, S., Jørgensen, J. K., & van Dishoeck, E. F. 2010, ApJ, 716, 825

Occhiogrosso, A., Viti, S., Modica, P., & Palumbo, M. E. 2011, MNRAS, 418, 1923

Vasyunin, A. I. & Herbst, E. 2013, ApJ, 762, 86

Vasyunin, A. I., Semenov, D., Henning, T., Wakelam, V., Herbst, E., & Sobolev, A. M. 2008, *ApJ*, 672, 629

Vasyunin, A. I., Sobolev, A. M., Wiebe, D. S., & Semenov, D. A. 2004, *Astronomy Letters*, 30, 566

Wakelam, V. & Herbst, E. 2008, *ApJ*, 680, 371

Wakelam, V., Herbst, E., Le Bourlot, J., Hersant, F., Selsis, F., & Guilloteau, S. 2010, *A&A*, 517, A21

Watanabe, N. & Kouchi, A. 2002, *ApJ*, 571, L173

Woon, D. E. & Herbst, E. 2009, *ApJS*, 185, 273

Table 1: New and Other Important Gas-phase Chemical Reactions

New Reaction	$\alpha$	$\beta$	$\gamma$	Temperature range (K)	Reference
$\text{CH}_3\text{O} + \text{H} \rightarrow \text{CH}_3 + \text{OH}$	1.6(-10)	0.0	0.0	300—2000	NIST
$\text{CH}_3\text{O} + \text{O} \rightarrow \text{H}_2\text{CO} + \text{OH}$	1.0(-10)	0.0	0.0	300—2500	NIST
$\text{CH}_3\text{O} + \text{CH}_3 \rightarrow \text{H}_2\text{CO} + \text{CH}_4$	4.0(-11)	0.0	0.0	300—2500	NIST
$\text{CH}_3\text{O} + \text{CH}_3 \rightarrow \text{CH}_3\text{OCH}_3 + \text{h}\nu$	1.0(-15)	-3.0	0.0	100—300	This work
Reaction	$\alpha$	$\beta$	$\gamma$	Temperature range (K)	Reference
$\text{CH}_3^+ + \text{CO} \rightarrow \text{C}_2\text{H}_3\text{O}^+ + \text{h}\nu$	1.2(-13)	-1.3	0.0	10—100	Herbst (1985)
$\text{O} + \text{C}_2\text{H}_3 \rightarrow \text{CH}_2\text{CO} + \text{H}$	1.6(-10)	0.0	0.0	10—2500	NIST
$\text{O} + \text{C}_2\text{H}_5 \rightarrow \text{CH}_3\text{CHO} + \text{H}$	1.33(-10)	0.0	0.0	10—2500	NIST
$\text{H}_3^+ + \text{CH}_3\text{OH} \rightarrow \text{CH}_3^+ + \text{H}_2\text{O} + \text{H}_2$	1.8(-9)	-0.5	0.0	100—1000	Woon & Herbst (2009)
$\text{CH}_3\text{OH}_2^+ + \text{CH}_3\text{OH} \rightarrow \text{CH}_3\text{OHCH}_3^+ + \text{H}_2\text{O}$	1.0(-10)	-1.0	0.0	100—300	Anicich et al. (2003)
$\text{H}_2\text{COH}^+ + \text{H}_2\text{CO} \rightarrow \text{H}_2\text{COHOCH}_2^+ + \text{h}\nu$	8.1(-15)	-3.0	0.0	10—300	Horn et al. (2004)
$\text{CH}_3^+ + \text{HCOOH} \rightarrow \text{HC(OH)}\text{OCH}_3^+ + \text{h}\nu$	1.0(-11)	-1.5	0.0	10—300	Garrod & Herbst (2006)
$\text{CH}_3\text{OH} + \text{OH} \rightarrow \text{CH}_3\text{O} + \text{H}_2\text{O}$	4.0(-11)	0.0	0.0	10—100	Cernicharo et al. (2012)

Notes: a(-b) stands for  $a \times 10^{-b}$ .  $\alpha$ ,  $\beta$  and  $\gamma$  are the coefficients in the modified Arrhenius expression for the reaction rate coefficient:  $k = \alpha \cdot (T/300)^\beta \cdot \exp(-\gamma/T)$ . URL for NIST Chemical Kinetics Database: <http://kinetics.nist.gov/kinetics/index.jsp>

Table 2: Observed and best-fit modeled fractional abundances of organic species detected in cold interstellar clouds

Species	M1		M10		Observations	
	L1689b	B1-b	L1689b	B1-b	L1689b	B1-b
HCOOCH <sub>3</sub>	4.9(-16)	4.2(-15)	3.3(-12)	2.0(-12)	7.4(-10) B	2.0(-11) C
CH <sub>3</sub> OCH <sub>3</sub>	2.4(-17)	1.8(-12)	1.3(-10)	3.7(-12)	1.3(-10) B	2.0(-11) C
CH <sub>3</sub> CHO	3.2(-11)	4.7(-12)	6.4(-11)	3.7(-11)	1.7(-10) B	1.0(-11) C
CH <sub>2</sub> CO	4.4(-11)	9.0(-12)	8.3(-11)	3.2(-11)	2.0(-10) B	1.3(-11) C
CH <sub>3</sub> O	5.3(-14)	8.5(-11)	8.5(-10)	1.5(-10)	—	4.7(-12) C
H <sub>2</sub> CO	9.8(-10)	2.9(-09)	5.4(-08)	4.8(-08)	1.3(-09) B	4.0(-10) M
CH <sub>3</sub> OH	5.7(-12)	2.5(-09)	2.3(-08)	3.3(-09)	-	3.1(-09) O

Notes: a(-b) stands for  $a \times 10^{-b}$ . B refers to Bacmann et al. (2012), C refers to Cernicharo et al. (2012), M refers to Marcelino et al. (2005), and O refers to Öberg et al. (2010). Times of best fits: Model M1:  $1.3 \times 10^5$  yr with L1689b,  $1.0 \times 10^6$  yr with B1-b, Model M10:  $5.1 \times 10^5$  yr with L1689b,  $2.6 \times 10^5$  yr with B1-b.

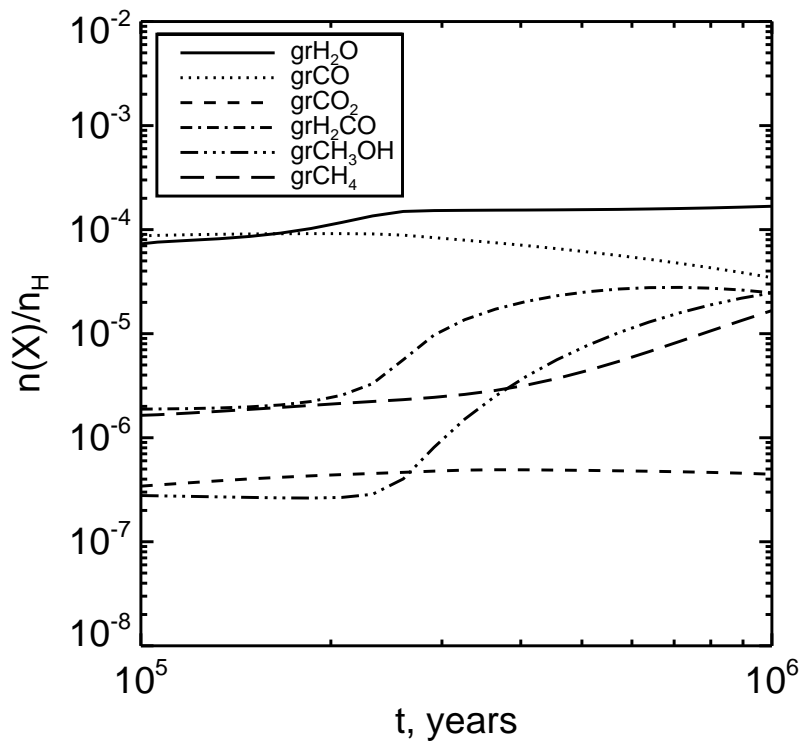


Fig. 1.— Abundances vs. time of water and major carbon-bearing ice compounds in the model M10. The prefix “gr” denotes species on and in ice mantles of interstellar grains.

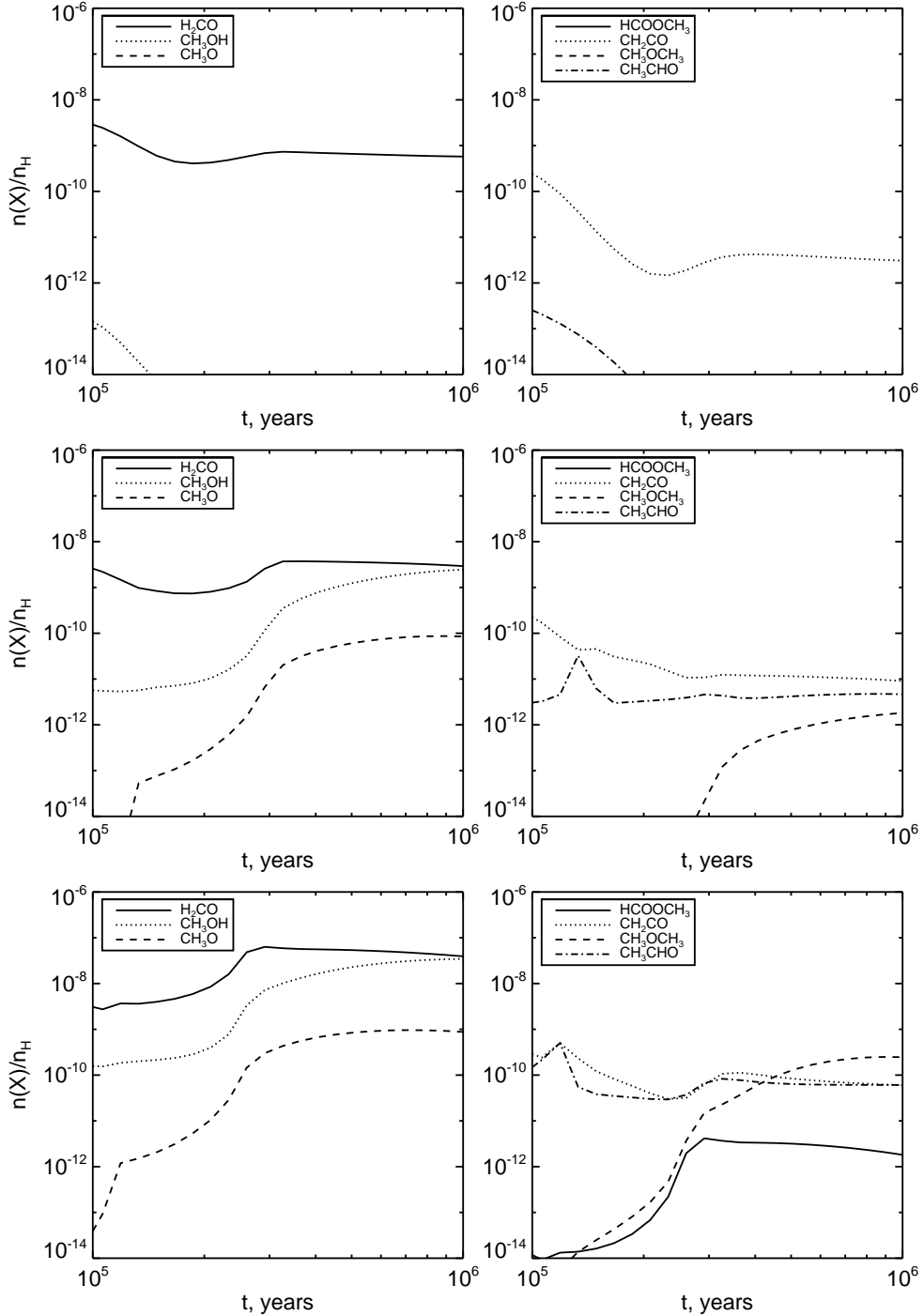


Fig. 2.— Gas-phase abundances vs time for simple and complex organic species in models M0 (top row), M1 (middle row), and M10 (bottom row).

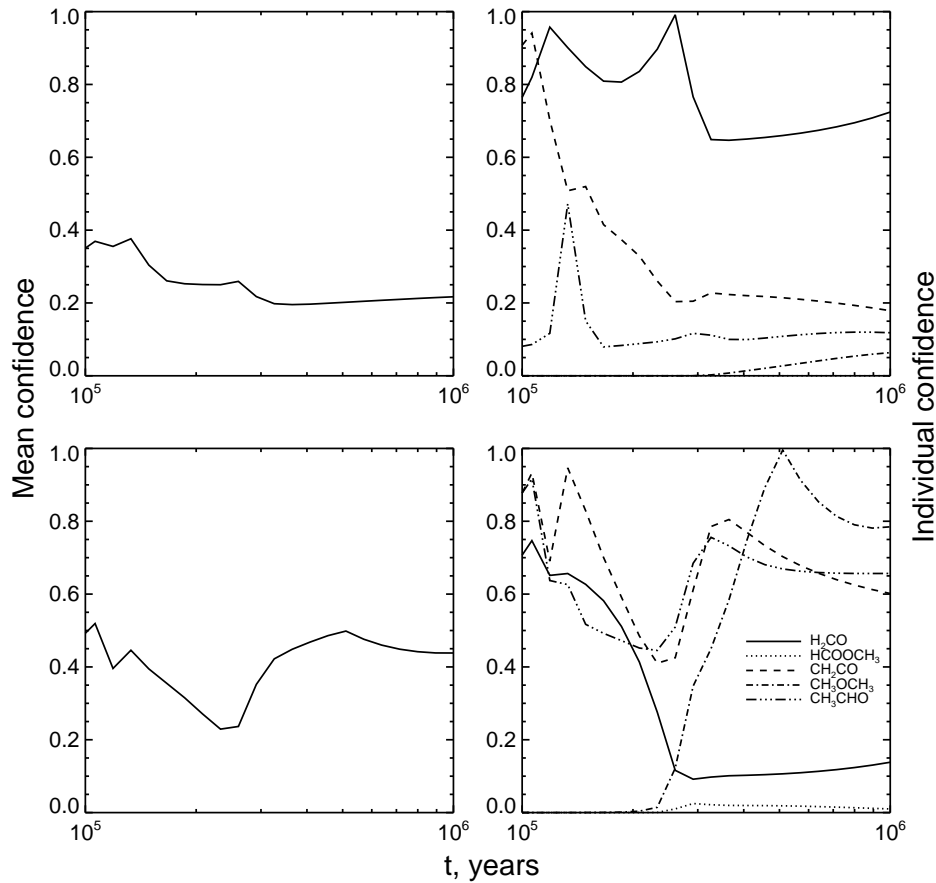


Fig. 3.— Mean and individual confidence levels for the species in models M1 (upper panels) and M10 (lower panels) in the case of L1689b. The higher the mean confidence level, the better the agreement between modeled and observed abundances.

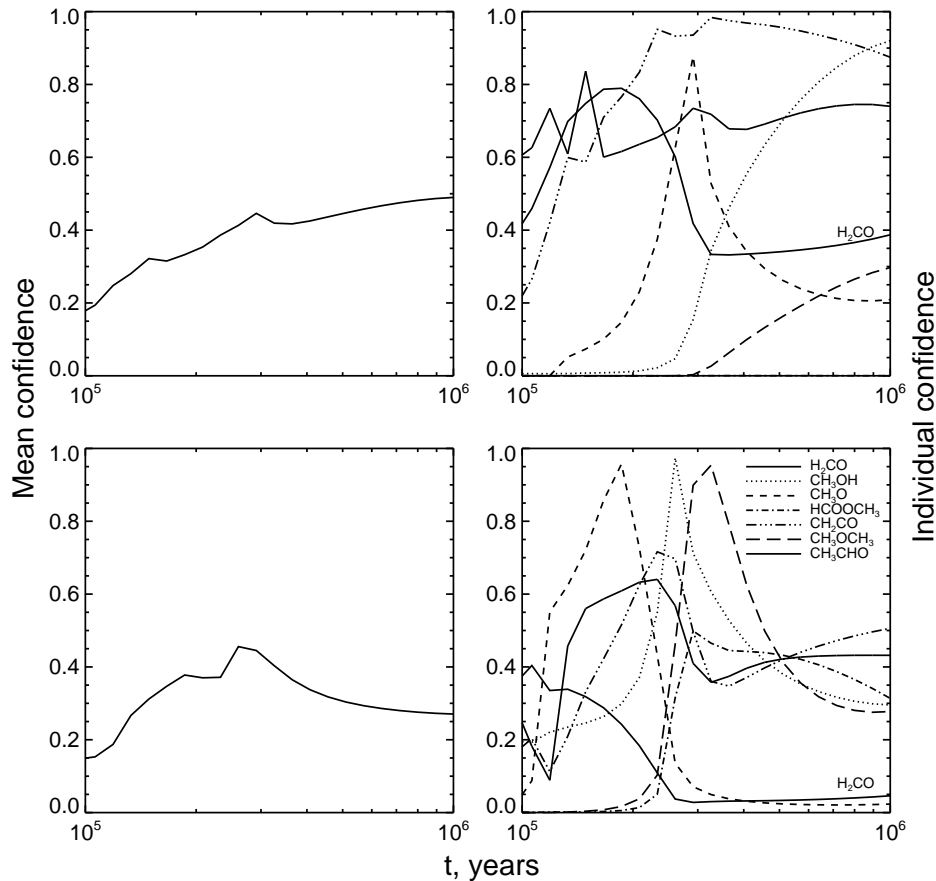


Fig. 4.— Mean and individual confidence levels for the species in models M1 (upper panels) and M10 (lower panels) in the case of B1-b. The higher the mean confidence level, the better the agreement between modeled and observed abundances.

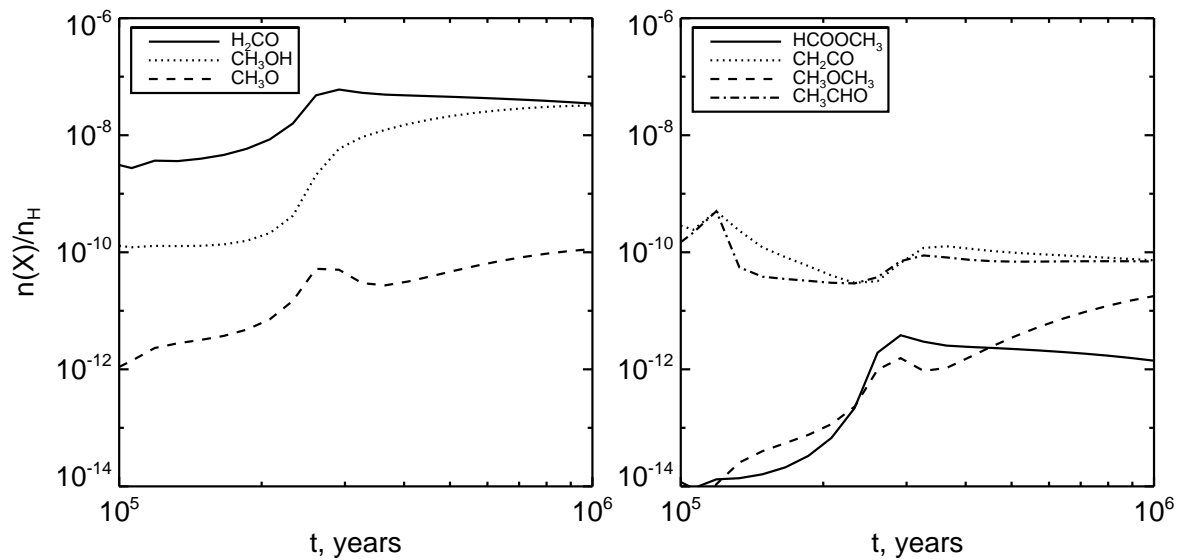


Fig. 5.— Abundances vs time of complex organic species and their precursors in the altered model M10, with reactive desorption of methoxy radicals switched off and reaction (13) enabled.